Pergamon

Oxygen isotopic compositions of IVA iron meteorites: Implications for the thermal evolution derived from in situ ultraviolet laser microprobe analyses

PEI-LING WANG,[1,*] DOUGLAS RUMBLE, III,[1] and TIMOTHY J. MCCOY[2]

[1]Geophysical Laboratory, Carnegie Institution of Washington, 5251 Broad Branch Road NW, Washington, DC 20015, USA
[2]National Museum of Natural History, Smithsonian Institution, Washington, DC 20560, USA

Abstract—Oxygen isotopic compositions of silicate inclusions in IVA iron meteorites have been measured with an in situ UV laser microprobe technique. The homogeneity of oxygen isotopic compositions within and among individual mineral grains has also been examined. Oxygen isotope fractionations between coexisting mineral pairs were utilized in oxygen isotope thermometry. Our measured $\Delta^{17}O$ values, ranging from 0.97 to 1.25‰, are characteristic of a single reservoir and fully confirm the oxygen isotopic similarity between IVA irons and L/LL chondrites. Steinbach and São João Nepomuceno, containing inclusions of two silicate minerals in mutual contact, exhibit a mass-dependent fractionation of $^{18}O/^{16}O$ between tridymite and bronzite with apparent oxygen isotopic heterogeneity. The SiO_2-bearing member, Gibeon, gives homogeneous oxygen isotopic compositions without detectable fractionation of $^{18}O/^{16}O$ between tridymite and quartz. Oxygen isotope equilibrium temperatures are estimated for coexisting tridymite and bronzite in the same sample slabs or clusters in Steinbach and São João Nepomuceno. The fractionations of $^{18}O/^{16}O$ between bronzite and tridymite range from 1.6 to 2.3‰ in different sample slabs or clusters. On the basis of the closure temperature concept, cooling rates are estimated at approximately 20 to 1000°C/Myr between 800 and 1000°C, a range of temperatures not accessible to other cooling rate methods. Using the Fast Grain Boundary diffusion model, we have demonstrated that significant oxygen heterogeneity both in tridymite and bronzite is probably due to isotope exchange during cooling between minerals with various grain sizes and mineral abundances in different regions of the samples. The new estimates of cooling rate by oxygen isotope thermometry refine previous cooling curves of IVA irons and support the breakup-reassembly model for the IVA parent body. *Copyright © 2004 Elsevier Ltd*

1. INTRODUCTION

Oxygen isotope systematics measured on scales from mineral grains to planets are a powerful geochemical tool to distinguish planetary and nebular processes and to test whether or not a group of meteorites originated from the same or different planetary bodies (Clayton, 1993). Oxygen isotopic analyses of silicate inclusions in iron meteorites can also be used to reconstruct parental planetary bodies from metal-rich cores to silicate mantles. Previous oxygen isotope measurements of silicate inclusions in IVA iron meteorites, including Steinbach, São João Nepomuceno, Gibeon and Bishop Canyon, demonstrated a similarity in oxygen isotopic composition between silicates in IVA irons and L or LL chondrites (Clayton and Mayeda, 1996).

The IVA iron meteorites consist of an Fe-Ni metal matrix with inclusions of bronzite, tridymite, and troilite. The accessory minerals have a grain size of approximately 1 mm and occur either as individual grains or as clusters of grains. The IVA iron meteorites are the third largest group of magmatic iron meteorites having chemical properties consistent with fractional crystallization of a single asteroidal core (Scott, 1972; Scott et al., 1996).

Petrographic and mineral chemistry considerations suggest the silicate inclusions were igneous cumulates, which crystallized from magmas of unusual silica-saturated composition (Ulff-Møller et al., 1995). The mixing of metal with silicates

may be due to shrinkage of the core upon solidification or a giant impact event (Ulff-Møller et al., 1995; Scott et al., 1996).

IVA irons exhibit a wide range of metallographic cooling rates from tens to thousands of °C per million years (Moren and Goldstein, 1979; Rasmussen et al., 1995), apparently conflicting with the hypothesis of a single core origin. Several models have been proposed to resolve the contradictory evidence. A raisin-bread model for the parental asteroid by Moren and Goldstein (1979) was provided to explain the span of cooling rates. The possibility of two parent bodies was raised because the cooling for high-Ni IVA irons is apparently slower than that for low-Ni IVA irons (Rasmussen, 1982). However, these hypotheses are inconsistent with measured trends of trace element fractional crystallization, which support an origin in the core of a single parent body (Scott et al., 1996; Wasson and Richardson, 2001). An alternative model suggested that the IVA parent body was catastrophically fragmented and reassembled after core crystallization but before formation of Widmanstätten intergrowths (Scott et al., 1994). The catastrophic breakup event is consistent with a fairly rapid cooling of Steinbach above 1000°C based on the equilibrium of its mineral assemblage (Reid et al., 1974). Microstructural observations further indicated that this meteorite was rapidly cooled at 100°C/h through 1200°C and at <300°C/yr in the range 1200 to 1000°C (Haack et al., 1996). Diverse metallographic cooling rates of IVA irons in the temperature range from 650 to 350°C may have resulted from thermal equilibration during and after reaccretion of fragmented materials in the reassembled asteroid (Rasmussen et al., 1995).

---

* Author to whom correspondence should be addressed (p.wang@gl.ciw.edu).

The reliability of metallographic cooling rate estimates is still under debate, however (Wasson and Richardson, 2001). A constant cooling rate for IVA irons over the interval 650 to 350°C may be derived by taking into account uncertainties in the location of equilibrium phase boundaries and in the magnitude of diffusion coefficients. Similar metallographic features between high-Ni and low-Ni IVA irons imply limited variation in cooling rates for IVA irons (Willis and Wasson, 1978). An observed correlation between metallographic cooling rate and composition may demonstrate a systematic error in the model used to estimate cooling rates (Wasson and Richardson, 2001).

An independent estimate of cooling rates below 650°C has been made by measurements of cation ordering in orthopyroxene from Steinbach and Sãn Jão Nepomuceno (Ganguly and Stimpfl, 2000). The new estimates agree in detail with none of the previous cooling rates, however. Assuming that both metal and silicates experienced similar thermal histories, an effort was made to bring into concordance both metallographic and cation ordering cooling rates. The effort succeeds if the statistical error limits in both estimates are stretched towards one another (Ganguly and Stimpfl, 2000). In view of these uncertainties and controversies, improvements in methods of calculating cooling rates are necessary. Caution should be exercised in accepting an evolutionary model that relies on inconclusive estimates of cooling rates for IVA irons. Indeed, the lack of cooling data between 1000 and 650°C imposes uncertainty on the whole pattern of cooling rate vs. temperature. It is this temperature interval, undocumented in previous studies, which will be addressed herein.

Measurements of oxygen isotope fractionations between minerals have been used extensively for geothermometry and 'geospeedometry' in terrestrial rocks. In this paper we follow these precedents in using $^{18}O/^{16}O$ fractionations to fill in the blank of IVA cooling history. Clayton and Mayeda (1996) reported an oxygen isotope equilibrium temperature of ~800°C based on a measured 2.5‰ fractionation of $^{18}O/^{16}O$ between bronzite in São João Nepomuceno and tridymite in Gibeon. Oxygen isotope analyses of mineral pairs coexisting in the same meteorite were not obtained, however.

The lack of oxygen isotope data for unraveling the cooling history of IVA irons stems from limits of sample size and spatial resolution imposed by earlier analytical methods. We have measured $\delta^{18}O$ and $\delta^{17}O$ compositions of coexisting mineral pairs from the same meteorite sample and used the data to estimate their oxygen isotope equilibrium temperatures directly. The simple mineralogy of IVA silicate inclusions with their millimeter grain size is particularly suitable for the ultraviolet (UV) laser microprobe technique which offers in situ, spatially-resolved analyses of individual mineral grains as small as 0.5 mm in diameter and high precision analysis for both $\delta^{17}O$ and $\delta^{18}O$ (±0.1‰) (Wiechert and Hoefs, 1995; Rumble et al., 1997).

Since low oxygen yields are associated with the use of a KrF UV laser (248 nm wavelength) during analysis of quartz (Wiechert and Hoefs, 1995), we performed analyses of tridymite with an ArF (193 nm) laser for comparison. A previous study indicated that better analytical results for quartz were realized with an ArF laser which generated a higher oxygen yield (Fiebig et al., 1999). Our study is the first to test the behavior of tridymite under these two different laser wavelengths. Complementary analyses of separated grains of tridymite and bronzite were conducted with a CO_2 laser to validate the use of an ArF laser for in situ analysis.

2. SAMPLES AND EXPERIMENTAL PROCEDURES

Sawn and polished slabs of the silicate-bearing IVA irons, Steinbach (USNM 3248), São João Nepomuceno (USNM 6881), Gibeon (USNM 6853) and Bishop Canyon (USNM 770) were selected for oxygen isotope analysis. The bronzite-tridymite-rich IVA irons, Steinbach and São João Nepomuceno, are composed of bronzite, tridymite, and troilite inclusions in Fe, Ni metal. Reported modal abundances for pyroxene are 66% of total silicate in Steinbach and 88% in São João Nepomuceno (Ulff-Møller et al., 1995; Scott et al., 1996). Because silicate inclusions occur in isolated clusters surrounded by Fe-Ni metal, modal proportions vary locally from 57 to 80% pyroxene in Steinbach, and 80 to 97% in São João Nepomuceno. The grain sizes of silicate minerals are varied and typically ~1 to 5 mm in Steinbach and São João Nepomuceno. The SiO_2-bearing IVA irons, Gibeon and Bishop Canyon, contain large, centimeter-size, but very rare silica grains. Cathodoluminescence observation shows a Gibeon inclusion to be dominantly composed of tridymite with a cracked area of quartz in its center, whereas Bishop Canyon contains pure tridymite grains (Marvin et al., 1997).

The 2 to 3 mm thick slabs were cleaned ultrasonically in de-ionized, distilled water, loaded into a reaction chamber with isotope reference minerals, heated under vacuum overnight to remove moisture, and then repeatedly fluorinated with purified F_2 until oxygen blanks were reduced to an acceptably low level. Blank levels were measured after fluorination by removing fluorine over heated KBr and observing the pressure of remaining noncondensable gases. In practice, acceptable blank levels were defined by the absence from the reaction chamber of noncondensable gases as measured on a 10 torr, 3 decimal place MKS Baratron capacitance manometer. Blanks were also monitored by analyses of isotope reference minerals loaded with meteorites in the reaction chamber.

The lasers used at the Geophysical Laboratory for mineral analyses were a Lambda-Physik Compex 110 excimer laser and a Synrad Series 48 CO_2 laser. The excimer laser can be filled with either a gas mixture of Kr-F_2-Ne giving 248 nm light or Ar-F_2-Ne giving 193 nm light. The CO_2 laser emits infrared light (IR) at a wavelength of 10.6 μm. Use of two different UV wavelengths for photo-ablation and a far IR wavelength for thermal ablation together with repeated analysis of isotope reference minerals provides a means for analytical validation. In situ analyses of 300 to 500 μm spots were performed by KrF and ArF excimer lasers. To avoid mixing oxygen from underlying minerals and to obtain the minimum amount of oxygen necessary for mass spectrometry, we accumulated the gas from several shallow, adjacent laser craters, instead of a single deep hole. The results were tested by analyzing hand-picked grains from Steinbach with a CO_2 laser. The in situ UV laser microprobe consists of an optical system for delivering and focusing the laser beam on the sample surface, a reaction chamber and vacuum extraction line with fluorine generator (Asprey, 1976), and a MAT 252 mass spectrometer. Samples are ablated in the reaction chamber through a UV-grade quartz glass window

Table 1. Effects on $\Delta^{17}O$ and $\delta^{18}O$ values of choosing different lasers to analyze silicate inclusions in IVA iron meteorites.[a]

Laser	$\delta^{18}O$ (‰)			$\Delta^{17}O$ (‰)		
	KrF	ArF	CO_2	KrF	ArF	CO_2
Steinbach (USNM 3248)						
Bronzite	3.89 ± 0.18	3.80 ± 0.33	4.06 ± 0.08	1.19 ± 0.03	1.24 ± 0.03	1.28 ± 0.08
Tridymite	6.43 ± 0.25	5.54 ± 0.38	5.34 ± 0.24	1.00 ± 0.08	1.20 ± 0.02	1.28 ± 0.04
São João Nepomuceno (USNM 6881)						
Bronzite	3.96 ± 0.12	3.98 ± 0.16		1.23 ± 0.03	1.27 ± 0.04	
Tridymite	7.09 ± 0.09	5.97 ± 0.37		1.02 ± 0.07	1.18 ± 0.05	

[a] Data are shown as an average $\pm$ standard deviation.

under a fluorine pressure of 20 torr with a laser energy fluence of over 8 J/cm^2. Excess fluorine is reacted with KBr to produce bromine at 110°C and the bromine is frozen in liquid nitrogen cold traps with other condensable gases. Oxygen is trapped in a cold finger with granules of molecular sieve substrate frozen with liquid nitrogen, isolated, heated to 80°C, and expanded through a crimped metal capillary directly into the ion source of the mass spectrometer (Rumble et al., 1997; Farquhar and Rumble, 1998). The CO_2 laser system uses BrF_5 as the reagent and omits the use of KBr but is otherwise similar to the UV laser system (Rumble and Hoering, 1994).

Due to the simple mineralogy and coarse grain size, it was possible to identify target minerals under a video microscope during in situ analyses. Mixing effects due to subjacent mineral grains unwittingly intersected in laser craters were carefully evaluated using optical microscopy and an electron microprobe analyzer following laser ablation. Roughness of laser ablation craters serves as a good indicator to distinguish bronzite and tridymite: laser ablation of bronzite generated rounded and smooth craters, while craters in tridymite were broken and fractured. Changes in F_2 pressure during laser ablation are diagnostic of which minerals are being ablated: pressure drops are associated with metal-bearing silicates because of the formation of solid metal fluorides; fluorination of silica polymorphs, however, produces gaseous products (SiF_4 and O_2). All mixture data were excluded.

Interlaboratory garnet and olivine reference materials, UWG-2 garnet with $\delta^{18}O = 5.8$‰ and San Carlos olivine with $\delta^{18}O = 5.2$‰ (Valley et al., 1995; Farquhar and Rumble, 1998), were loaded and analyzed with every meteorite sample. The two reference materials were used both for in situ analysis with the excimer laser and for analysis of chips and powders with the CO_2 laser. Raw values of $\delta^{18}O$ were corrected to give the accepted values for these reference minerals. Calculation of $\Delta^{17}O$ from measured $\delta^{18}O$ and $\delta^{17}O$ values was based on direct measurement of a mass-dependent, terrestrial fractionation line following Miller's (2002) suggestion. Our mass-dependent terrestrial fractionation line is defined by 298 analyses of silicate and oxide minerals with a wide range of $\delta^{18}O$ values from -15 to 10‰. The slope of our measured terrestrial fractionation line is 0.5225 with an intercept of -0.1206‰ and an R^2 of 0.99999. The analytical uncertainties with both the excimer and CO_2 laser systems in measurement of $\delta^{18}O$ and $\Delta^{17}O$ values produce standard deviations of 0.1 and 0.05‰, respectively.

3. RESULTS

3.1. Laser-Induced Isotope Fractionation in Tridymite Analysis

Ablation accuracy of the two available UV wavelengths, 248 nm and 193 nm, was assessed by direct comparison with CO_2 laser results to obtain the most accurate oxygen isotope measurements. Interlaboratory comparisons have established CO_2 laser analyses of silicates for oxygen isotopes as the primary criterion for validating excimer laser results (Valley et al., 1995; Wiechert and Hoefs, 1995; Rumble et al., 1997). Analyses of bronzite give similar $\delta^{18}O$ and $\Delta^{17}O$ values no matter which UV wavelength was used (Table 1). No laser-induced isotope fractionation has been observed in the analysis of bronzite. On the contrary, however, tridymite analyses show systematic differences in both $\delta^{18}O$ and $\Delta^{17}O$ depending on which laser was used. Analytical results for both ArF and CO_2 lasers are in mutual agreement but results with KrF are 1‰ too high for $\delta^{18}O$ values and 0.2‰ too low for $\Delta^{17}O$ values (Table 1). We conclude that the ArF laser is the correct choice for in situ analysis of tridymite but the choice between ArF and KrF lasers is arbitrary for in situ pyroxene analysis (Fiebig et al., 1999). Oxygen isotopic compositions of tridymite measured using KrF laser were excluded in further discussions.

3.2. Oxygen Isotopic Composition of IVA Irons

Oxygen isotopic compositions of silicate mineral inclusions in IVA iron meteorites are listed in Table 2 and plotted on a three-isotope diagram (Fig. 1). Previous data are plotted for comparison (Clayton and Mayeda, 1996). Values of $\Delta^{17}O$ from Steinbach are 1.22 ± 0.05‰ (n = 15) for bronzite and 1.25 ± 0.05‰ (n = 7) for tridymite. São João Nepomuceno has $\Delta^{17}O$ values of 1.24 ± 0.04‰ (n = 24) for bronzite and 1.18 ± 0.05‰ (n = 2) for tridymite. Values of $\Delta^{17}O$ from Gibeon are 1.07 ± 0.03‰ (n = 5) for tridymite and 0.97‰ (n = 1) for quartz. Bishop Canyon has $\Delta^{17}O$ values of 1.10 ± 0.04‰ for tridymite (n = 8). The mean $\Delta^{17}O$ value for IVA silicates is 1.16 ± 0.09‰ from our laser ablation analysis, essentially identical to that previously determined from bulk analysis (1.17 ± 0.11‰) (Clayton and Mayeda, 1996).

The bronzite-tridymite-bearing IVA irons exhibit mass-dependent fractionation of $\delta^{17}O$ and $\delta^{18}O$ between tridymite and bronzite with the minerals plotting in a linear array parallel to the terrestrial fractionation line (Fig. 1). The data are consistent

Table 2. Oxygen isotopic compositions of silicate inclusions in IVA iron meteorites.

Sample slabs	Cluster-grain-analysis	Mineral	Technique	δ^{18}O (‰)	δ^{17}O (‰)	Δ^{17}O (‰)
			Steinbach(USNM3248)			
STB-1	A-a-1	bronzite	KrF laser	3.86	3.19	1.17
	A-b-1	bronzite	KrF laser	3.86	3.22	1.21
	A-b-2	bronzite	KrF laser	3.90	3.16	1.12
	A-c-1	bronzite	KrF laser	3.68	3.11	1.19
	A-c-2	bronzite	KrF laser	3.75	3.18	1.22
			average (s.d.)	3.81 (0.09)	3.17 (0.04)	1.18 (0.04)
	B-a-1	bronzite	KrF laser	4.22	3.41	1.21
	B-a-2	bronzite	KrF laser	4.11	3.36	1.21
			average (s.d.)	4.16 (0.07)	3.39 (0.04)	1.21 (0.00)
STB-2A	A-a-1	bronzite	ArF laser	4.07	3.37	1.25
	A-a-2	bronzite	ArF laser	4.20	3.43	1.24
	A-a-3	bronzite	ArF laser	3.70	3.13	1.20
	A-b-1	bronzite	ArF laser	3.62	3.17	1.28
	A-c-1	bronzite	KrF laser	3.77	3.17	1.20
	A-d-1	bronzite	ArF laser	3.41	3.03	1.25
			average (s.d.)	3.80 (0.29)	3.22 (0.15)	1.24 (0.03)
	A-e-1	tridymite	ArF laser	5.69	4.20	1.22
	A-f-1	tridymite	ArF laser	5.82	4.26	1.22
	A-g-1	tridymite	ArF laser	5.11	3.85	1.18
			average (s.d.)	5.54 (0.38)	4.10 (0.22)	1.21 (0.02)
STB	*bulk*	*bronzite*	*CO_2 laser*	*4.01*	*3.31*	*1.22*
	bulk	*bronzite*	*CO_2 laser*	*4.12*	*3.48*	*1.33*
			average (s.d.)	*4.06 (0.08)*	*3.40 (0.12)*	*1.28 (0.08)*
	bulk	*tridymite*	*CO_2 laser*	*5.36*	*4.10*	*1.30*
	bulk	*tridymite*	*CO_2 laser*	*5.28*	*3.98*	*1.22*
	bulk	*tridymite*	*CO_2 laser*	*5.65*	*4.24*	*1.29*
	bulk	*tridymite*	*CO_2 laser*	*5.08*	*3.96*	*1.31*
			average (s.d.)	*5.34 (0.24)*	*4.07 (0.13)*	*1.28 (0.04)*
			São João Nepomuceno (USNM 6881)			
SJN-1	A-a-1	bronzite	KrF laser	3.96	3.32	1.25
	A-a-2	bronzite	KrF laser	3.86	3.25	1.23
	A-a-3	bronzite	KrF laser	3.90	3.25	1.21
	A-b-1	bronzite	KrF laser	4.13	3.37	1.22
	A-c-1	bronzite	KrF laser	3.83	3.22	1.22
	A-c-2	bronzite	KrF laser	3.92	3.29	1.24
	A-d-1	bronzite	KrF laser	3.84	3.28	1.28
	A-d-2	bronzite	KrF laser	3.92	3.32	1.27
	A-d-3	bronzite	KrF laser	4.13	3.33	1.17
	A-d-4	bronzite	KrF laser	4.13	3.39	1.23
	A-e-1	bronzite	KrF laser	4.02	3.30	1.20
	A-f-1	bronzite	KrF laser	4.01	3.31	1.22
	A-f-2	bronzite	KrF laser	4.01	3.35	1.26
			average (s.d.)	3.97 (0.11)	3.31 (0.05)	1.23 (0.03)
SJN-2B	A-a-1	bronzite	KrF laser	3.98	3.26	1.18
	A-b-1	bronzite	ArF laser	3.93	3.35	1.30
	A-c-1	bronzite	KrF laser	3.82	3.27	1.27
	A-c-2	bronzite	ArF laser	3.82	3.25	1.25
			average (s.d.)	3.89 (0.08)	3.28 (0.05)	1.25 (0.05)
	A-d-1	tridymite	ArF laser	6.23	4.40	1.15
			Steinbach (USNM 3248)			
SJN-3A	A-a-1	bronzite	KrF laser	3.86	3.27	1.25
	B-a-1	bronzite	KrF laser	3.77	3.24	1.27
	B-b-1	bronzite	KrF laser	4.15	3.35	1.18
	B-b-2	bronzite	ArF laser	3.96	3.38	1.31
			average (s.d.)	3.93 (0.16)	3.31 (0.07)	1.26 (0.06)
	C-a-1	bronzite	KrF laser	3.97	3.29	1.22
	C-a-2	bronzite	KrF laser	4.04	3.34	1.23
	C-b-1	bronzite	ArF laser	4.21	3.43	1.23
			average (s.d.)	4.07 (0.12)	3.35 (0.07)	1.23 (0.01)
	C-d-1	tridymite	ArF laser	5.71	4.20	1.21
			Gibeon (USNM 6853)			
GB	A-a-1	tridymite	ArF laser	7.00	4.72	1.06
	A-a-2	tridymite	ArF laser	6.89	4.67	1.07
	A-a-3	tridymite	ArF laser	6.83	4.68	1.11
	A-a-4	tridymite	ArF laser	6.99	4.74	1.09
	A-a-5	tridymite	ArF laser	7.07	4.73	1.04
			average (s.d.)	6.95 (0.10)	4.71 (0.03)	1.07 (0.03)
	A-b-1	quartz	ArF laser	6.89	4.57	0.97

Table 2. (Continued)

Sample slabs	Cluster-grain-analysis	Mineral	Technique	$\delta^{18}O$ (‰)	$\delta^{17}O$ (‰)	$\Delta^{17}O$ (‰)
			Bishop Canyon (USNM 770)			
BC	A-a-1	tridymite	ArF laser	4.22	3.32	1.12
	A-a-2	tridymite	ArF laser	5.32	3.84	1.06
	A-a-3	tridymite	ArF laser	5.82	4.15	1.11
	A-a-4	tridymite	ArF laser	4.97	3.71	1.11
	A-a-5	tridymite	ArF laser	4.80	3.58	1.07
	A-a-6	tridymite	ArF laser	4.32	3.40	1.14
	A-a-7	tridymite	ArF laser	4.23	3.24	1.03
	A-a-8	tridymite	ArF laser	3.78	3.13	1.16
		average (s.d.)		4.68 (0.67)	3.55 (0.34)	1.10 (0.04)

Data with CO_2 laser analysis are in italic to distinguish from those with UV laser.

with a model of parent body accretion and homogenization followed by mass-dependent fractionation. Oxygen isotopic heterogeneity within individual samples was observed. Steinbach has $\delta^{18}O$ values of tridymite from 5.0 to 5.8‰ and bronzite is 3.4 to 4.2‰ with averages of 5.4 ± 0.3‰ (n = 7) and 3.9 ± 0.2‰ (n = 15), respectively. Tridymite $\delta^{18}O$ values from São João Nepomuceno are 5.7 to 6.2‰ and bronzite from 3.8 to 4.2‰ averaging 6.0 ± 0.4‰ (n = 2) and 4.0 ± 0.1‰ (n = 24), respectively. The distribution of $\delta^{18}O$ values and the corresponding minerals of Steinbach and São João Nepomuceno are plotted in Figures 2 and 3. Almost identical $\delta^{18}O$ values derived from different lasers in a single bronzite grain are shown in slabs SJN-2B and SJN-3A (Fig. 3). Homogeneity of $\delta^{18}O$ within a cluster of contiguous grains is greater than that between clusters separated from one another. For example, in the two clusters illustrated for slab STB-1 (Fig. 2), pyroxene in

the cluster on the left has an average of 3.8 ± 0.1‰ whereas it is 4.2 ± 0.1‰ on the right.

The IVA irons that contain SiO_2 as the only silicate phase show different features (Fig. 4). Gibeon has homogeneous $\delta^{18}O$ values of 7.0 ± 0.1‰ (n = 5) for tridymite and no significant difference of $\delta^{18}O$ values was measured between tridymite and quartz, within error (Fig. 4a). However, tridymite $\delta^{18}O$ values from Bishop Canyon are highly heterogeneous ranging from 3.8 to 5.8‰ with no apparent systematic spatial distribution (Fig. 4b). The $\delta^{18}O$ values obtained in this study are generally consistent with those from Clayton and Mayeda (1996) except for Bishop Canyon. Given the highly heterogeneous $\delta^{18}O$ values from Bishop Canyon observed here, however, we might expect some difference between our values for Bishop Canyon and that of Clayton and Mayeda (1996), which utilized a different sample.
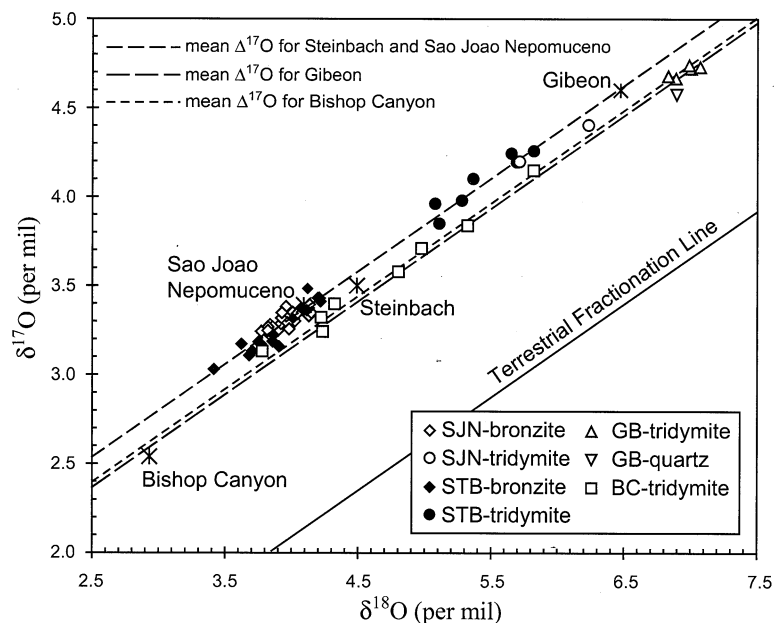

Fig. 1. Three oxygen isotope plot of IVA silicates. The terrestrial fractionation line is shown for reference. Data from Steinbach (STB) and São João Nepomuceno (SJN) fall on a secondary mass-dependent fractionation trend with $\Delta^{17}O$ value of 1.23‰. Data from Gibeon (GB) and Bishop Canyon (BC) fall on lines with $\Delta^{17}O$ value of 1.06‰ and 1.10‰ respectively. Stars indicate the data with bulk analyses by Clayton and Mayeda (1996).
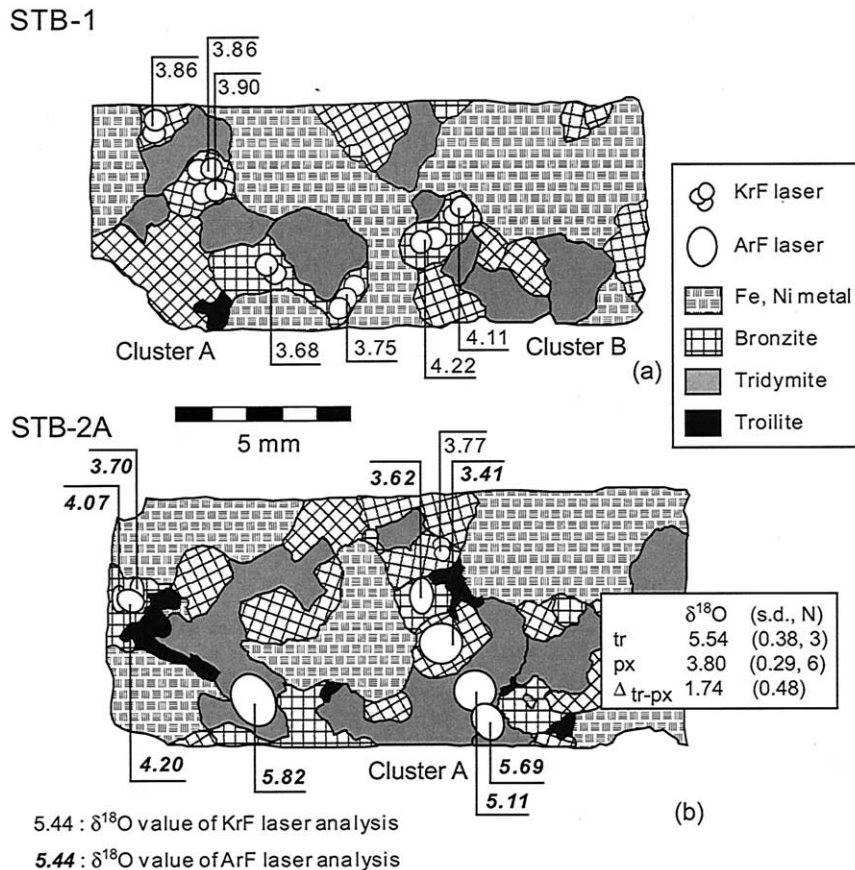
Fig. 2. Mineral and $\delta^{18}O$ map of Steinbach. KrF laser analyses of bronzite are shown as multiple circles indicating several laser ablation craters for one analysis and the $\delta^{18}O$ values are in plain text. ArF laser analyses are shown as a single ellipse covering an area with several laser ablation craters (not shown individually) and the $\delta^{18}O$ values are in bold italic text. KrF laser analyses of bronzite range from 3.7 to 4.2‰; ArF laser analyses are 3.4 to 4.2‰. Tridymite analyses with ArF laser are from 5.1 to 5.8‰. Averages and fractionation data for the sample slab or cluster are indicated aside.

4. DISCUSSION

4.1. Precursor of IVA Iron Meteorites

The $\Delta^{17}O$ results are similar to previous data with a range of from 1.02 to 1.26‰ (Clayton and Mayeda, 1996). Considering the analytical uncertainty, the values of $\Delta^{17}O$ of Steinbach and São João Nepomuceno are identical and notably greater than the values of Gibeon and Bishop Canyon, however, the ranges of data overlap (Fig. 5). It would be difficult to defend the grouping of the IVA iron meteorites into two different parent bodies, however. Not only are their metal compositions consistent with origin on a single body (Wasson and Richardson, 2001) but also the difference in $\Delta^{17}O$ values is small. Heterogeneity in oxygen isotopic compositions is not unusual within groups of achondrites: large variations of $\Delta^{17}O$ values have been noted among the ureilites (Clayton and Mayeda, 1996). It is a reasonable hypothesis that Bishop Canyon, for example, was isolated within the parent body and never equilibrated with other IVA silicates. We conclude that the small variations in $\Delta^{17}O$ values among IVA silicates result from incomplete homogenization during parent body accretion, heating, and differentiation.

Our measured $\Delta^{17}O$ values fully confirm the similarity in oxygen isotopic compositions between silicates in IVA irons and L or LL chondrites found in previous studies (Clayton et al., 1983). In comparison with the mean $\Delta^{17}O$ values of equilibrated L and LL chondrites (Clayton et al., 1991), Steinbach and São João Nepomuceno are more like LL chondrites and Gibeon and Bishop Canyon are closer to L chondrites. As mentioned above, however, there is no strong evidence to support the existence of two parent bodies for IVA irons. The mean $\Delta^{17}O$ value of IVA silicates is actually intermediate between that of L and LL chondrites (Fig. 5). It is not possible to choose between L and LL chondrites or link them separately as the precursor of IVA irons. Oxygen isotope data establishes a possible genetic linkage between L or LL chondrites and IVA iron meteorites, but other types of data are needed to confirm their association.

4.2. Oxygen Isotope Thermometry

4.2.1. Estimates of equilibrium temperature

The origin of silicate phases in IVA iron meteorites as igneous cumulates in a magma derived by high degrees of partial melting from a chondritic precursor with subsequent
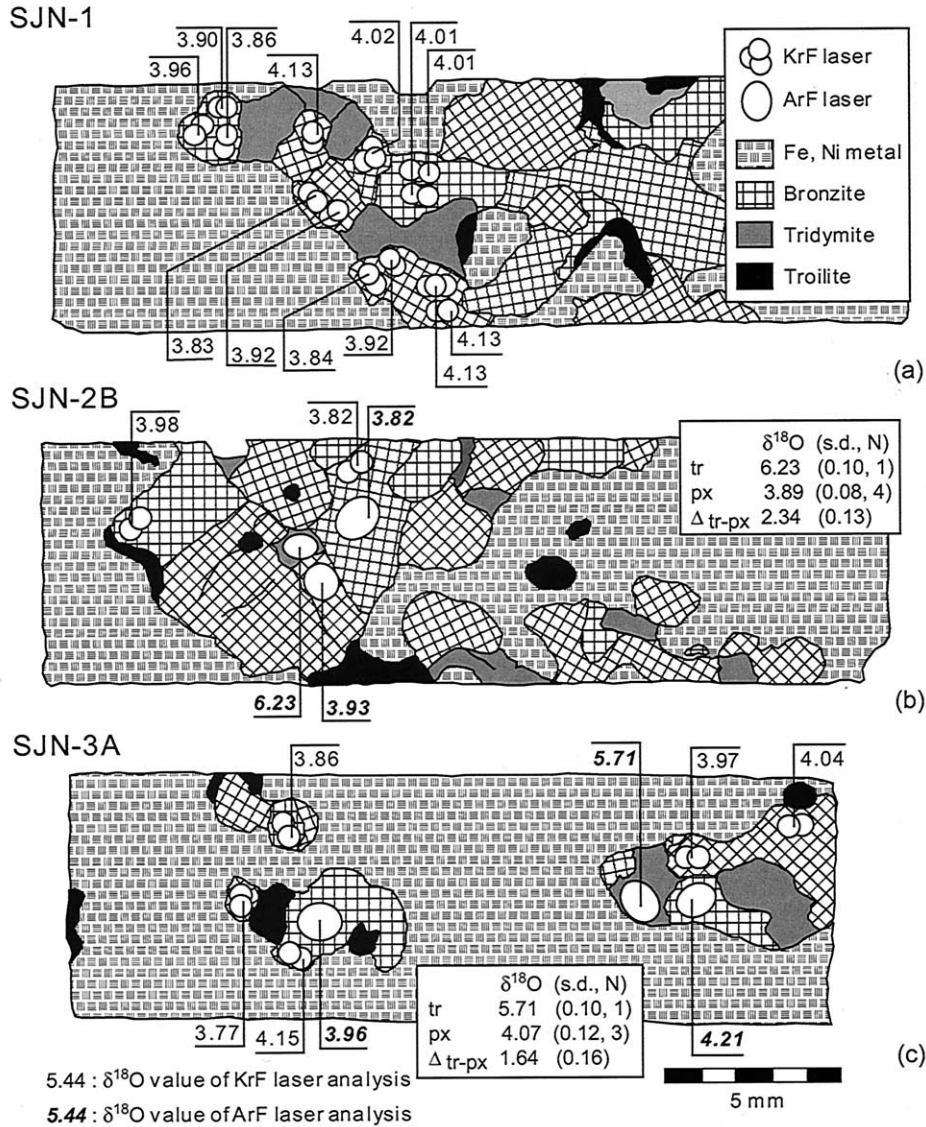
Fig. 3. Mineral and δ^{18}O map of São João Nepomuceno. Symbols and lettering are shown as in Figure 2. KrF laser analyses of bronzite range from 3.8 to 4.2‰; ArF laser analyses are 3.8 to 4.2‰. Tridymite analyses with ArF laser are from 5.7 to 6.2‰.

reduction of Fe has been proposed (Ulff-Møller et al., 1995). Metal and silicate phases were mixed at the core/mantle boundary by solidification shrinkage during parent body cooling (Ulff-Møller et al., 1995). Petrographic study of silicate-silicate grain boundaries confirmed that the silicates were co-crystallized (Scott et al., 1996). The application of oxygen isotope geothermometry is appropriate in such a system.

Due to the observed oxygen isotopic heterogeneity within individual samples, it would be meaningless to estimate equilibrium temperatures by taking the mean δ^{18}O values in each sample. Silicates isolated by surrounding metal may not have equilibrated with each other during crystallization nor exchanged isotopes during cooling. The fractionations of ^{18}O/^{16}O between bronzite and tridymite used for geothermometry were derived from adjacent mineral grains in the same slab or cluster (Table 3). The fractionation of ^{18}O/^{16}O between bronzite and

tridymite is ~1.7‰ in slab STB-2A for Steinbach and ~2.3 and 1.6‰ in slabs SJN-2B and SJN-3A for São João Nepomuceno, respectively. Equilibrium temperatures were estimated as between 800 and 1000°C (Table 3) on the basis of experimental calibration of the quartz-diopside pair (Chiba et al., 1989; Clayton and Kieffer, 1991). The errors of estimated equilibrium temperatures vary from 30 to 200°C depending on the uncertainties imposed by mineral heterogeneity on the small intermineral fractionations. Owing to the lack of experimental calibration of fractionation factor of tridymite and bronzite, both theoretical and increment calibrations were applied (Smyth and Clayton, 1988; Smyth, 1989; Zheng, 1993a,b). The temperature estimates increase by 40 to 80°C systematically, if the increment or theoretical fractionations between tridymite and ferrosilite are applied (Table 3). The discrepancies in temperature estimates arising from the use of different calibrations are
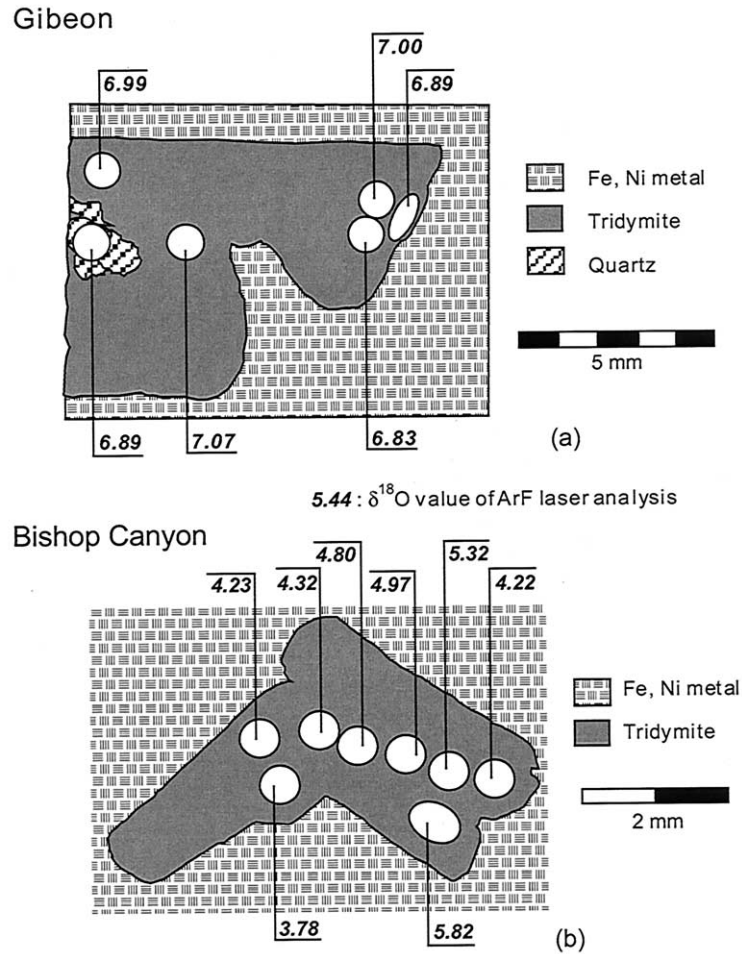
Fig. 4. Mineral and $\delta^{18}O$ map of Gibeon and Bishop Canyon. All analyses were performed with ArF laser. A circle represents an analysis covering an area with several laser ablation craters. Tridymite and retrograde quartz in Gibeon have the same oxygen isotope composition, but tridymite from Bishop Canyon is heterogeneous in $^{18}O/^{16}O$.

smaller than the errors derived from the uncertainties of measured fractionations in bronzite-tridymite pairs.

The measured zero fractionation of $^{18}O/^{16}O$ between tridymite and quartz stands in contrast to the 'reasonable' temperature estimates based on oxygen isotope partitioning between tridymite and pyroxene. Tridymite-quartz fractionations of less than 0.1‰ correspond to a ridiculously high equilibrium temperature of over 1650°C (Smyth and Clayton, 1988; Smyth, 1989; Zheng, 1993b). The two minerals could not have stably coexisted at such a high temperature because it is above the quartz-tridymite transition temperature of 870°C (Marvin et al., 1997). Therefore, an estimate of oxygen equilibrium temperature for Gibeon would be meaningless. Our measurements of identical $\delta^{18}O$ values for coexisting tridymite and quartz in Gibeon shows that there was no fractionation of $^{18}O/^{16}O$ during the polymorphic inversion of tridymite to quartz and subsequent cooling.

4.2.2. Estimates of cooling rate with the closure temperature theory

In theory, equilibrium temperature can only be estimated correctly when two or more coexisting minerals achieve equilibrium under a stationary temperature condition. Oxygen isotope equilibrium is difficult to attain and hard to prove, however, because rocks cool down along a temperature-time path. In practice, oxygen isotope exchange is a kinetic process and dominated by inter and intracrystalline diffusion. Diffusion-driven isotope exchange effectively ceases below a specific temperature, the closure temperature (Tc), which is defined as:

$$Tc = \frac{E/R}{\ln\left[\dfrac{ARTc^2 D_0/a^2}{E(dT/dt)}\right]}$$

where a is diffusion size, E is activation energy, R is the gas constant, A is diffusion geometry factor, D_0 is preexponential factor of diffusivity, and dT/dt is cooling rate (Dodson, 1973). For a given mineral, Tc is higher for larger grain sizes and fast cooling rates. In a two-mineral assemblage, oxygen isotopes will stop exchanging when the system cools down to a temperature equal to the higher Tc of the two minerals (Giletti, 1986; Jenkin et al., 1994). If this specific isotopic composition is maintained without further disturbance, the oxygen isotope equilibrium temperature estimated from the $^{18}O/^{16}O$ fraction-
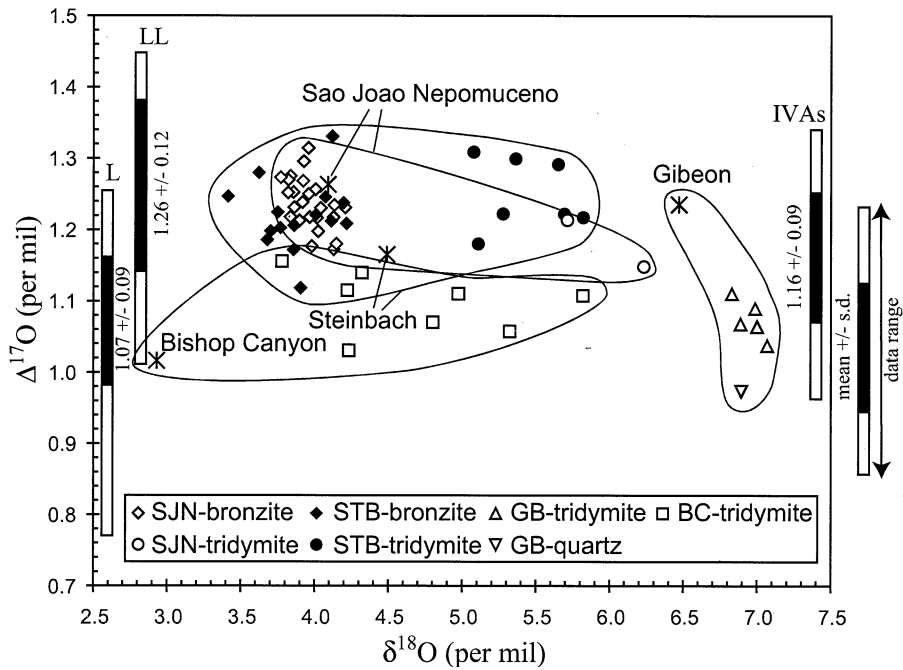
Fig. 5. Plot of $\Delta^{17}O$ values against $\delta^{18}O$ values for IVA silicates. Stars indicate the data for IVA silicates with bulk analyses by Clayton and Mayeda (1996). Data for equilibrated L and LL chondrites are shown with bars for comparison (data from Clayton et al., 1991). Black bars indicate the mean values for different group of meteorites and white bars below the black show the whole range of the data.

ation of the mineral pair would equal the Tc of the first closure mineral.

In our case, pyroxene with a lower diffusion coefficient has a higher Tc than tridymite and stops diffusive exchange first during cooling (Giletti and Yund, 1984; Farver, 1989). The oxygen isotope temperature of a pyroxene-tridymite pair represents the Tc of pyroxene at defined grain size and cooling rate. Conversely, the cooling rate can be derived if the Tc and grain size are known. Using available diffusion parameters

(Giletti and Yund, 1984; Farver, 1989) and a measured grain size of 2 mm, cooling rates were estimated at 976°C/Myr at 984°C of slab STB-2A in Steinbach, 23°C/Myr at 811°C of slab SJN-2B and 1945°C/Myr at 1022°C of slab SJN-3A in São João Nepomuceno. Apparently, different sample slabs record different cooling rates at different temperatures.

Uncertainties in the four parameters involved in the calculation of Tc are responsible for discrepancies in cooling rate estimates. The uncertainty in Tc derived from an error in the

Table 3. Oxygen isotope equilibrium temperatures for IVA iron meteorites.

Method	Mineral	$\delta^{18}O$ (‰)[a]	N[b]	$\delta^{18}O_{Tr}-\delta^{18}O_{Py}$ (‰)[a]	Teq_{Q-Di} (°C)[a,c,e]	$Teq_{Tr-Ferr}$ (°C)[d,e]
				Steinbach		
Laser ablation STB-2A	Tridymite	5.54 ± 0.38	3			
	Bronzite	3.80 ± 0.29	6	1.74 ± 0.48	984 ± 181	1058/1028
				São João Nepomuceno		
Laser ablation SJN-2B	Tridymite	6.23 ± 0.10	1			
	Bronzite	3.89 ± 0.08	4	2.34 ± 0.13	811 ± 30	875/853
Laser ablation SJN-3A	Tridymite	5.71 ± 0.10	1			
	Bronzite	4.07 ± 0.12	3	1.64 ± 0.17	1022 ± 62	1098/1064
				IVA irons		
Bulk fluorination	Gibeon tr	6.47 ± 0.10	1			
	Bronzite	4.09 ± 0.10	2	2.38 ± 0.14	805 ± 32	865/843

[a] Data are shown as average ± standard deviation. An uncertainty of 0.10‰ has been assigned for single analysis.

[b] N = Number of analyses.

[c] Teq (°C)$_{Q-Di}$ is estimated by experimental calculations of fractionation factors (Chiba et al., 1989). Quartz-diopside, $1000 \ln \alpha = 2.75 \times 10^6/T^2$. Error propagation for quartz-diopside thermometer, $T = 2.75^{0.5} \times 10^3 \times \Delta^{-0.5} = 1658 \times \Delta^{-0.5}$, err $T = 1658 \times 0.5 \times$ err $\Delta \times \Delta^{-1.5}$.

[d] Teq (°C)$_{Tr-Ferr}$ is estimated by theoretical estimates of fractionation factors. Two sets of fractionation factors are used for the estimates. The estimates before and after the slash are based on fractionation factors by theoretical and increment methods respectively (Smyth and Clayton, 1988; Smyth, 1989; Zheng, 1993a,b).

[e] Data and Teq are estimated by Clayton and Mayeda (1996). Tridymite is from Gibeon and bronzite is from São João Nepomuceno. Errors for $\delta^{18}O$ measurements are assumed to be 0.10‰.

Table 4. Summary of cooling rate data for IVA iron meteorites.

Method	Sample	T range (°C)	Cooling rate
Cpx microtexture[a] (uncertainty of cooling rate is unknown)			
	Steinbach	1200	100°C/hr
Troilite nodule[a] (uncertainty of cooling rate is unknown)			
	Steinbach	1200–1000	<300°C/yr
Oxygen isotope thermometry[b] (uncertainty of cooling rate is better than a factor of 2)			
	Steinbach (STB-2A)	984 ± 173	976°C/Myr
	São João Nepomuceno (SJN-2B)	811 ± 30	23°C/Myr
	São João Nepomuceno (SJN-3A)	1022 ± 62	1945°C/Myr
Widmanstätten pattern[c] (uncertainty of cooling rate is better than a factor of 3)			
	Steinbach	650–450/450–350	150/20°C/Myr
	São João Nepomuceno	650–350	890°C/Myr
Metallographic texture[d] (uncertainty of cooling rate is a factor of 2)			
	IVA irons	650–350	109°C/Myr
Cation ordering in orthopyroxene[e] (uncertainty of cooling rate is a factor of 5 to 10)			
	Steinbach	473–429	40347–2267°C/Myr
	São João Nepomuceno	409–396	558–200°C/Myr
Compromise between metallographic and cation ordering cooling rates[e]			
	Steinbach	470–430/<425	400/50°C/Myr
	São João Nepomuceno	400	400°C/Myr

[a] Data from Haack et al. (1996).
[b] Data from this study.
[c] Data from Rasmussen et al. (1995).
[d] Data from Wasson and Richardson (2001).
[e] Data from Ganguly and Stimpfl (2000).

activation energy of 5 kcal/mol (E = 54 ± 5 kcal/mol) would be around 100°C, which is greater than the error in equilibrium temperature for a homogeneous cluster, such as SJN-2B and SJN-3A. Considering the error on activation energy and assigning an uncertainty on grain size as 50%, cooling rate estimates are known to better than a factor of 2 for an inhomogeneous cluster, such as STB-2A. The closure temperature model of Dodson (1973), itself, is limited in its applicability, because intracrystalline volume diffusion is considered in only one of the two minerals and isotopic exchange between the two minerals is ignored.

4.2.3. Variation of oxygen compositions with the fast grain boundary diffusion model

We have applied a more realistic approach than Dodson's (1973) model to calculating oxygen isotope exchange between minerals in IVA silicates using the Fast Grain Boundary (FGB) model (Eiler et al., 1992; Eiler et al., 1993) to investigate oxygen isotope heterogeneity within and among sample slabs and mineral grain clusters. The FGB model describes a portion of a rock in which grain boundaries continuously maintain isotopic equilibrium during a change in temperature with time. Transportation and exchange of oxygen follow three rules at any moment during cooling: Diffusivity of oxygen is controlled by volume diffusion within crystals; isotopic equilibrium is always maintained in grain boundaries; and the whole system is mass conserved meaning that the inflow and outflow of oxygen isotopes from different minerals is balanced. The FGB model includes parameters like fractionation between minerals and modal abundance not considered in Dodson's (1973) equation. Trial calculations were performed using a range of input values of cooling rate, grain size, and modal abundance to estimate the sensitivity of oxygen isotopes and Tc to these variables.

Numerical sensitivity tests computed with the FGB model showed that variations in both grain size and modal abundance could account for the observed heterogeneity in $\delta^{18}O$ in IVA silicates. Taking a pyroxene abundance of 66% for Steinbach, computed variations in $\delta^{18}O$ for a given cooling rate were around 0.3‰ for quartz and 0.2‰ for pyroxene over a range in grain sizes of 1 to 5 mm. Variations in $\delta^{18}O$ for São João Nepomuceno were around 0.4 to 0.5‰ for quartz and less than 0.1‰ for pyroxene with 88% pyroxene. Performing a different set of calculations to test sensitivity in relation to modal abundances, larger variations in $\delta^{18}O$ were found than for changes in grain sizes. For Steinbach with 57 to 80% pyroxene, values of $\delta^{18}O$ in minerals changed by as much as 0.5‰. São João Nepomuceno with 80 to 97% pyroxene showed changes of 0.3 to 0.4‰. Increasing cooling rates decreased $\delta^{18}O$ variations slightly. We conclude that a combination of variations in both grain sizes and modal abundances can explain observed heterogeneity in $\delta^{18}O$ in minerals of IVA irons. The variations in grain size and mineral mode are seen on the scale of individual silicate grain clusters in the Fe-Ni metal matrix.

Fractionation of $^{18}O/^{16}O$ and Tc computed with the FGB model were consistent with measured fractionations and oxygen isotope equilibrium temperatures. Cooling rate estimates calculated with the FGB model, however, were systematically slower than those derived from Dodson's equation, but they agree within the uncertainty.

4.3. Thermal Evolution of IVA Iron Meteorites

The thermal evolution of IVA iron meteorites presented below was derived from published cooling rate data estimated by different methods and in this study (Table 4). Assuming their origin in an asteroidal core of a differentiated body, IVA irons probably cooled at a rate in the range of 100 to 1000°C/Myr during crystallization (Wood, 1979). Observation with a
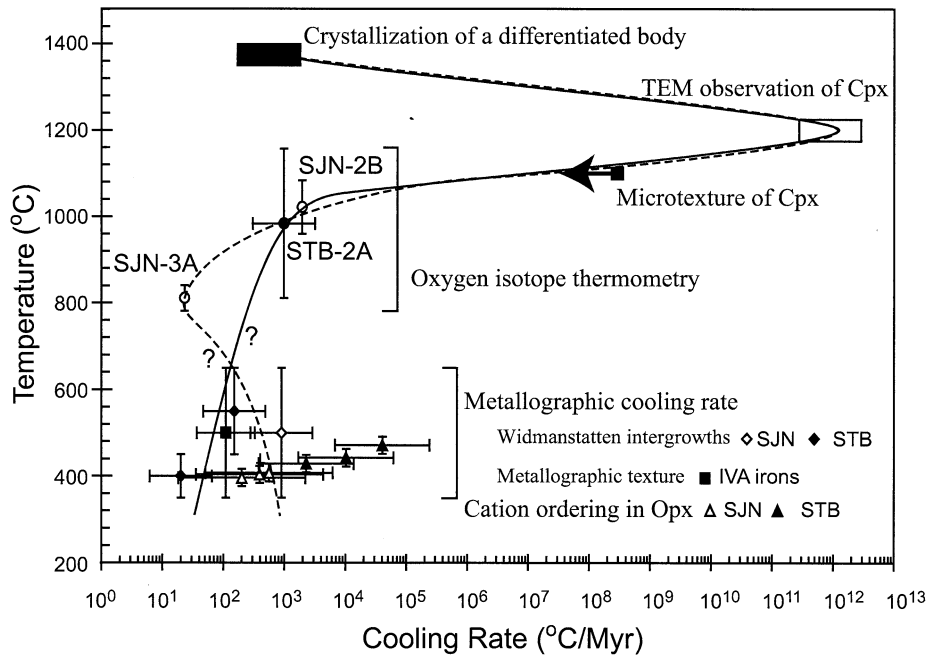
Fig. 6. Summary of cooling rate estimates with corresponding temperature ranges for IVA iron meteorites. The data are listed in table 4 (Wood, 1979; Haack et al., 1996; Rasmussen et al., 1996; Ganguly and Stimpfl, 2000; Wasson and Richardson, 2001). An arrow represents the data only with the upper limit estimate. Dashed and solid curves show the change of cooling rates through the temperatures for Steinbach and São João Nepomuceno. A dramatic increase in cooling rates at around 1200°C followed by a decrease derived from oxygen isotope thermometry is observed apparently.

TEM of disordered clinobronzite in Steinbach indicated a cooling rate of 100°C/h at 1200°C (Haack et al., 1996). Absence of dendrites in large troilite nodules indicated a cooling rate was less then 300°C/yr in the range 1200 to 1000°C (Haack et al., 1996). Oxygen isotope thermometry in the present study gives estimates of cooling rates in the range between 1000 and 800°C, which fills the gap in previous estimates omitted by other methods. Steinbach cooled at 980°C/Myr. São João Nepomuceno shows a change in cooling from 1900 to 20°C/Myr with temperature decrease. Estimates of cooling rates below 650°C for IVA irons are still under debate. Cooling may have been highly varied based on the most recent Ni diffusion coefficients and Fe-Ni phase diagram (Rasmussen et al., 1995) or the rate may have been uniform as suggested by several similarities in metallographic features shared by different meteorites (Wasson and Richardson, 2001). Cation ordering states in orthopyroxene from Steinbach and São João Nepomuceno also provide cooling rate estimates below 650°C, but they are only consistent with metallographic cooling rates if the data are stretched to the limits of uncertainty for both estimates (Ganguly and Stimpfl, 2000).

The cooling rate estimates and conceptual cooling paths of IVA irons are plotted in Figure 6. Owing to disagreement between cooling rate estimates below 650°C, it is not possible to deduce distinguishable cooling paths for each meteorite from 800 to 650°C. A general pattern of cooling is evident, however. Accretion of the parent body led to heating, melting, and differentiation into mantle and core. Initial cooling during crystallization and solidification of the body was slow. This was followed by fast cooling, and then slow cooling again (Fig. 6). The dramatic increase in cooling rates at around 1200°C is

fairly strong evidence for the breakup event suggested by Haack et al. (1996) and this is shown conceptually in Figure 7 (Stage I to II). Following rapid cooling at ~1200°C, cooling rates slow at intermediate temperatures (~1000–800°C). The variations in cooling rates derived from oxygen isotope thermometry may be controlled by different local thermal environments, such as would be found in the reassembled rubble pile of mixed hot and cold fragments following the breakup (Fig. 7, Stage II to III). A steady state thermal regime may or may not have been reached in the reaccreted rubble pile in the temperature range ~650 to 350°C, depending upon whether uniform or various cooling rates are accepted (Rasmussen et al., 1995; Wasson and Richardson, 2001). The ^{40}K cosmic-ray exposure ages for IVA irons (Lavielle et al., 1999; Lavielle et al., 2001) suggest that the rubble pile was destroyed between 375 and 207 Ma (Fig. 7, Stage IV).

5. SUMMARY

An in situ UV laser microprobe technique for oxygen isotope analysis has been applied to four silicate-bearing IVA iron meteorites (Steinbach, São João Nepomuceno, Gibeon and Bishop Canyon). The laser ablation technique offers spatially-resolved analyses of individual mineral grains as small as 0.5 mm with an uncertainty of 0.1‰ for δ^{18}O and δ^{17}O values. Our results, showing oxygen isotopic heterogeneity on the scale of individual mineral grains and clusters of minerals, are summarized below.

1. Laser-induced isotope fractionation is observed between KrF and ArF lasers for tridymite analyses; however there is no difference between KrF and ArF lasers for bronzite analyses.
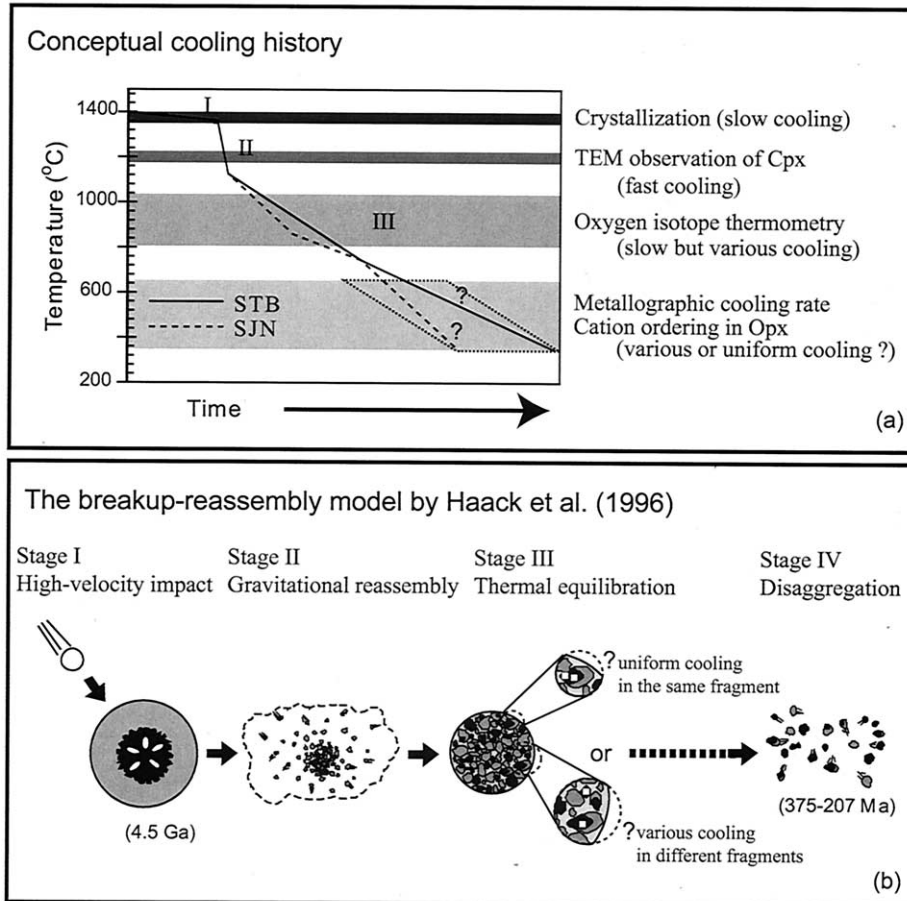
Fig. 7. (a) Conceptual cooling history for the IVA parent body and (b) schematic representation of the evolution model are plotted for correlation between cooling rate estimates and evolution stages. The evolution model is modified from the breakup-reassembly model proposed by Haack et al. (1996). Black is solid metal, white is liquid metal, and gray is silicate. Small white squares in stage III represent possible final sampling in IVA silicates, depending on cooling rate variation in lower temperature interval.

The consistency of data from ArF and CO_2 lasers for tridymite suggests that an ArF laser is more reliable than a KrF laser for in situ analyses of SiO_2 minerals.

2. The values of $\Delta^{17}O$ show a general consistency with previous data from bulk analyses. There is a small but distinguishable difference between the mean $\Delta^{17}O$ value for bronzite-tridymite-bearing members (Steinbach and São João Nepomuceno) and that for SiO_2-bearing members (Gibeon and Bishop Canyon). We do not advocate more than one parent body for IVA irons, however, because the compositions of the meteorites lie along a single fractional crystallization trend. Small differences in $\Delta^{17}O$ values may be due to incomplete homogenization within a heterogeneous parent body. Our measurements of $\Delta^{17}O$ values for silicate inclusions in IVA irons confirm a possible genetic linkage between IVA's and L/LL chondrites.

3. Bronzite-tridymite mineral pairs exhibit mass-dependent fractionation of $^{18}O/^{16}O$ with $\delta^{18}O$ heterogeneity of 0.8 to 0.4‰ among different clusters. The average $\delta^{18}O$ values of bronzite are 3.9 ± 0.2‰ in Steinbach and 4.0 ± 0.1‰ in São João Nepomuceno. For tridymite, they are 5.4 ± 0.3‰ and 6.0 ± 0.4‰ in Steinbach and in São João Nepomuceno, respec-

tively. Gibeon exhibits homogeneous $^{18}O/^{16}O$ composition without detectable difference in $\delta^{18}O$ between tridymite and quartz, which implies no fractionation of oxygen, neither during a partial phase change nor during subsequent cooling.

4. Based on measured fractionations of $^{18}O/^{16}O$ between bronzite and tridymite, equilibrium temperatures are estimated as approximately between 800 to 1000°C for different sample slabs or mineral grain clusters in Steinbach and São João Nepomuceno. The closure temperature concept further implies that the oxygen isotopic temperature would equal the Tc of bronzite in a bronzite-tridymite system. Cooling rates estimated with Dodson's equation have uncertainties of less than a factor of two. According to the FGB modeling, the oxygen isotopic heterogeneity in IVA silicates is probably due to variations in grain sizes and mineral abundances in local silicate mineral clusters isolated from each other by a Fe-Ni metal matrix. Cooling rates estimated with the FGB model are systematically lower than those calculated from Dodson's (1973) equation but the uncertainties of both calculations are mutually overlapping.

5. The estimates of cooling rates with oxygen isotope thermometry offer a unique constraint for cooling paths between 1000 and 800°C for IVA iron meteorites. Our results support

the breakup-reassembly model with a marked decrease and variation of cooling rates immediately after the breakup event. Due to uncertainties of cooling rate estimates below 650°C, it is impossible to characterize detailed cooling paths for different samples. Cooling rate variations with oxygen isotope thermometry may indicate localized thermal environments after breakup and reassembly of the parent body. Differences in burial depth of fragments in the reassembled parent body may have caused variations in cooling rates.

REFERENCES

Asprey L. B. (1976) The preparation of very pure fluorine gas. *J. Fluor. Chem.* **7,** 359–361.

Chiba H., Chacko T., Clayton R. N., and Goldsmith J. R. (1989) Oxygen isotope fractionations involving diopside, forsterite, magnetite, and calcite: Application to geothermometry. *Geochim. Cosmochim. Acta* **53,** 2985–2995.

Clayton R. N. (1993) Oxygen isotopes in meteorites. *Ann. Rev. Earth Planet. Sci.* **21,** 115–149.

Clayton R. N., Mayeda T. K., Olsen E. J., and Prinz M. (1983) Oxygen isotope relationships in iron meteorites. *Earth Planet. Sci. Lett.* **65,** 229–232.

Clayton R. N. and Kieffer S. W. (1991) Oxygen isotopic thermometer calibrations. In *Stable Isotope Geochemistry: A Tribute to Samuel Epstein* (eds. H. P. Taylor, J. R. O'Neil, and I. R. Kaplan), pp. 3–10. The Geochemical Society, Special Publication.

Clayton R. N., Mayeda T. K., Goswami J. N., and Olsen E. J. (1991) Oxygen isotope studies of ordinary chondrites. *Geochim. Cosmochim. Acta* **55,** 2317–2337.

Clayton R. N. and Mayeda T. K. (1996) Oxygen isotope studies of achondrites. *Geochim. Cosmochim. Acta* **60,** 1999–2017.

Dodson M. H. (1973) Closure temperature in cooling geochronological and petrologic systems. *Contrib. Mineral. Petrol.* **40,** 259–274.

Eiler J. M., Baumgartner L. P., and Valley J. W. (1992) Intercrystalline stable isotope diffusion: A fast grain boundary model. *Contrib. Mineral. Petrol.* **112,** 543–557.

Eiler J. M., Valley J. W., and Baumgartner L. P. (1993) A new look at stable isotope thermometry. *Geochim. Cosmochim. Acta* **57,** 2571–2583.

Farquhar J. and Rumble D. (1998) Comparison of oxygen isotope data obtained by laser fluorination of olivine with KrF excimer laser and CO_2 laser. *Geochim. Cosmochim. Acta* **62,** 3141–3149.

Farver J. R. (1989) Oxygen self-diffusion in diopside with application to cooling rate determinations. *Earth Planet. Sci. Lett.* **92,** 386–396.

Fiebig J., Wiechert U., Rumble D., and Hoefs J. (1999) High-precision in-situ oxygen isotope analysis of quartz using an ArF-laser. *Geochim. Cosmochim. Acta* **63,** 687–702.

Ganguly J. and Stimpfl M. (2000) Cation ordering in orthopyroxenes from two stony-iron meteorites: Implications for cooling rates and metal-silicate mixing. *Geochim. Cosmochim. Acta* **64,** 1291–1297.

Giletti B. J. (1986) Diffusion effects on oxygen isotope temperatures of slowly cooled igneous and metamorphic rocks. *Earth Planet. Sci. Lett.* **77,** 218–228.

Giletti B. J. and Yund R. A. (1984) Oxygen diffusion on quartz. *J. Geophy. Res.* **89,** 4039–4046.

Haack H., Scott E. R. D., Love S. G., Brearley A. J., and McCoy T. J. (1996) Thermal histories of IVA stony-iron and iron meteorites: Evidence for asteroid fragmentation and reaccretion. *Geochim. Cosmochim. Acta* **60,** 3103–3113.

Jenkin G. R. T., Farrow C. M., Fallick A. E., and Higgins D. (1994) Oxygen isotope exchange and closure temperatures in cooling rocks. *J. Metamorphic Geol.* **12,** 221–235.

Lavielle B., Marti K., Jeannot J.-P., Nishiizumi K., and Caffee M. (1999) The ^{36}Cl-^{36}Ar-^{40}K-^{41}K records and cosmic ray production rates in iron meteorites. *Earth Planet. Sci. Lett.* **170,** 93–104.

Lavielle B., Caffee M., Gilabert E., Nishiizumi K., and Ponganis K. (2001) Irradiation records in group IVA irons (abstract). *Meteorit. Planet. Sci.* **36,** A110.

Marvin U. B., Petaev M. I., Croft W. J., and Killgore M. (1997) Silica minerals in the Gibeon IVA iron meteorite. *Lunar Planet. Sci.* **28,** 879–880.

Miller M. F. (2002) Isotopic fractionation and the quantification of ^{17}O anomalies in the oxygen three-isotope system: An appraisal and geochemical significance. *Geochim. Cosmochim. Acta* **66,** 1881–1889.

Moren A. E. and Goldstein J. I. (1979) Cooling rates of group IVA iron meteorites determined from a ternary Fe-Ni-P model. *Earth Planet. Sci. Lett.* **43,** 182–196.

Rasmussen K. L. (1982) Determination of the cooling rates and nucleation histories of eight group IVA iron meteorites using local bulk Ni and P variation. *Icarus* **52,** 444–453.

Rasmussen K. L., Ulff-Møller F., and Haack H. (1995) The thermal evolution of IVA iron meteorites: Evidence from metallographic cooling rates. *Geochim. Cosmochim. Acta* **59,** 3049–3059.

Reid A. M., Williams R. J., and Takeda H. (1974) Coexisting bronzite and clinobronzite and the thermal evolution of the Steinbach meteorite. *Earth Planet. Sci. Lett.* **22,** 67–74.

Rumble D. and Hoering T. C. (1994) Analysis of oxygen and sulfur isotope ratios in oxide and sulfide minerals by spot heating with a CO_2 laser in a fluorine atmosphere. *Acct. Chem. Res.* **27,** 237–241.

Rumble D., Farquhar J., Young E. D., and Christensen C. P. (1997) In situ oxygen isotope analysis with an excimer laser using F_2 and BrF_5 reagents and O_2 gas as analyte. *Geochim. Cosmochim. Acta* **61,** 4229–4234.

Scott E. R. D. (1972) Chemical fractionation in iron meteorites and its interpretation. *Geochim. Cosmochim. Acta* **36,** 1205–1236.

Scott E. R. D., Brearley A. J., Haack H., and McCoy T. J. (1994) Catastrophic fragmentation and reassembly of the parent body of the IVA iron and stony-iron meteorites. *Meteoritics* **29,** 530–531.

Scott E. R. D., Haack H., and McCoy T. J. (1996) Core crystallization and silicate-metal mixing in the parent body of the IVA iron and stony-iron meteorites. *Geochim. Cosmochim. Acta* **60,** 1615–1631.

Smyth J. R. (1989) Electrostatic characterization of oxygen sites in minerals. *Geochim. Cosmochim. Acta* **53,** 1101–1110.

Smyth J. R. and Clayton R. N. (1988) Correlation of oxygen isotope fractionation and electrostatic site potentials in silicates. *Trans. Am. Geophys. Union* **69,** 1514.

Ulff-Møller F., Rasmussen K. L., Prinz M., Palme H., Spettel B., and Kallemeyn G. W. (1995) Magmatic activity on the IVA parent body: Evidence from silicate-bearing iron meteorites. *Geochim. Cosmochim. Acta* **59,** 4713–4728.

Valley J. W., Kitchen N., Kohn M. J., Niedorf C. R., and Spicuzza M. J. (1995) UWG-2, a garnet standard for oxygen isotope ratios: Strategies for high precision and accuracy with laser heating. *Geochim. Cosmochim. Acta* **59,** 5223–5231.

Wasson J. T. and Richardson J. W. (2001) Fractionation trends among IVA iron meteorites: Contrasts with IIIAB trends. *Geochim. Cosmochim. Acta* **65,** 951–970.

Wiechert U. and Hoefs J. (1995) An excimer laser-based micro analytical preparation technique for in-situ oxygen isotope analysis of silicate and oxide minerals. *Geochim. Cosmochim. Acta* **59,** 4093–4101.

Willis J. and Wasson J. T. (1978) A core origin for group IVA iron meteorites: A reply to Moren and Goldstein. *Earth Planet. Sci. Lett.* **40,** 162–167.

Wood J. A. (1979) Review of the metallographic cooling rates of meteorites and a new model for the planetesimals in which they formed. In *Asteroids* (ed. T. Gehrels), pp. 849–891. University of Arizona Press.

Zheng Y.-F. (1993a) Calculation of oxygen isotope fractionation in anhydrous silicate mineral. *Geochim. Cosmochim. Acta* **57,** 1079–1091.

Zheng Y.-F. (1993b) Oxygen isotope fractionation in SiO_2 and Al_2SiO_5 polymorphs: Effect of crystal structure. *Eur. J. Mineral.* **5,** 651–658.